**Structural Basis for Lipid-mediated Activation of G Protein-coupled Receptor GPR55**

Tobias Claff[1], Rebecca Ebenhoch[1], Jörg T. Kley[1], Aniket Magarkar[1], Herbert Nar[1], Dietmar Weichert[1]*

[1]*Boehringer Ingelheim Pharma GmbH & Co. KG, Global Medicinal Chemistry, Birkendorfer Str. 65, 88397 Biberach an der Riß*

**Corresponding author: dietmar.weichert@boehringer-ingelheim.com*

**Table of contents**

**Supplementary Figures**



**Supplementary Tables**

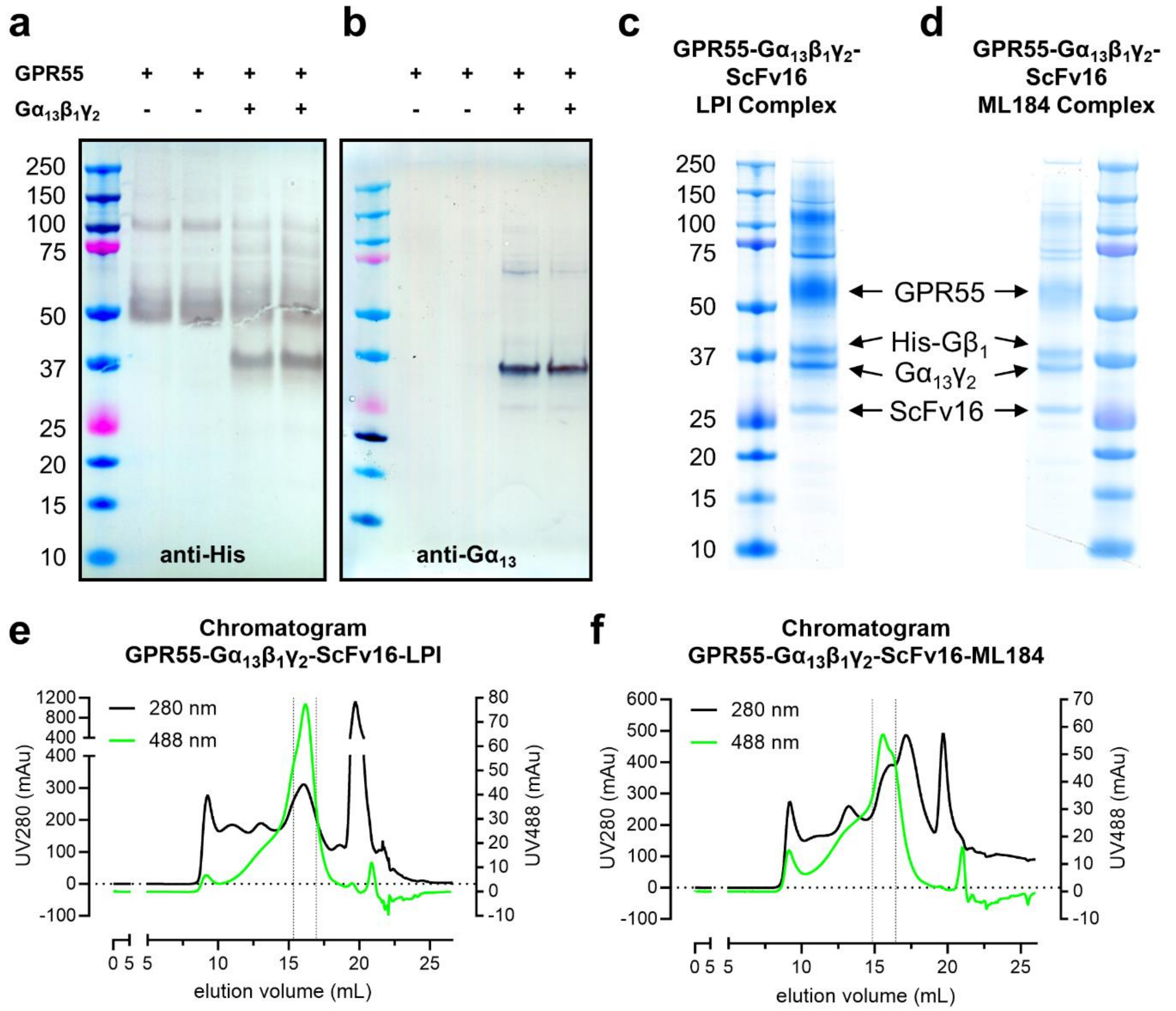


**Supplementary Fig. S1. Expression and purification of the GPR55-G$\alpha_{13}\beta_1\gamma_2$-ScFv16 complex with LPI and ML184. a** and **b** Western blot of Hi5 insect cell lysates expressing GPR55 alone or together with heterotrimeric G protein using **a** anti-His antibody or **b** anti-G$\alpha_{13}$ antibody. **c** and **d** SDS-PAGE analysis of the final protein used for cryo-EM grid preparation for the **c** GPR55-G$\alpha_{13}\beta_1\gamma_2$-ScFv16-LPI complex or **d** GPR55-G$\alpha_{13}\beta_1\gamma_2$-ScFv16-ML184 complex. **e** and **f** Chromatogram of the **e** GPR55-G$\alpha_{13}\beta_1\gamma_2$-ScFv16-LPI complex or **f** GPR55-G$\alpha_{13}\beta_1\gamma_2$-ScFv16-ML184 during purification using a Superose™ 6 Increase 10/300 GL column on an ÄKTA pure™ chromatography system (Cytiva) equipped with a 10 mm flow cell. Peak fractions for each complex were pooled according to the GFP absorption peak at 488 nm as indicated by vertical dotted lines.

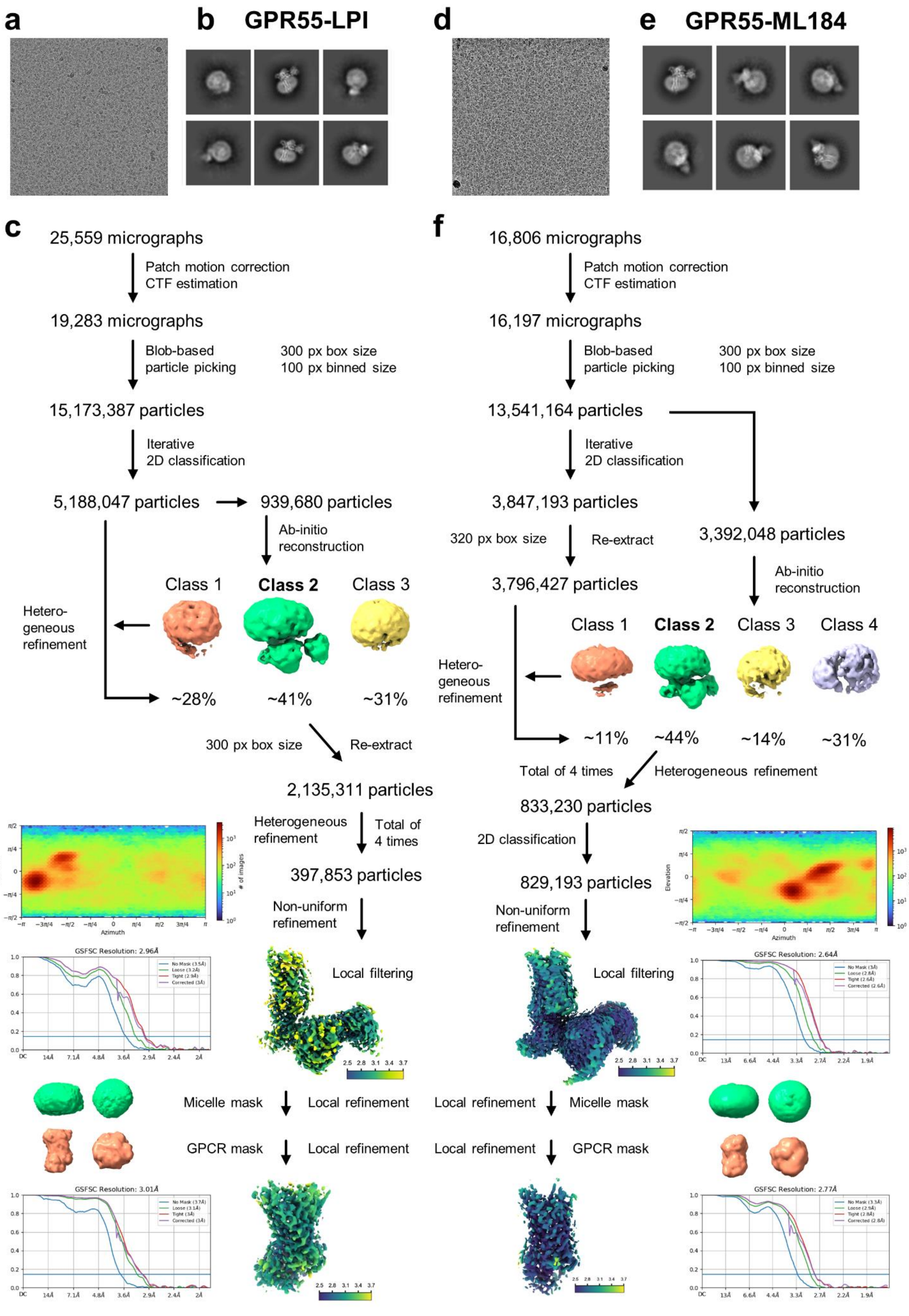


**Supplementary Fig. S2. Cryo-EM data processing workflow.**

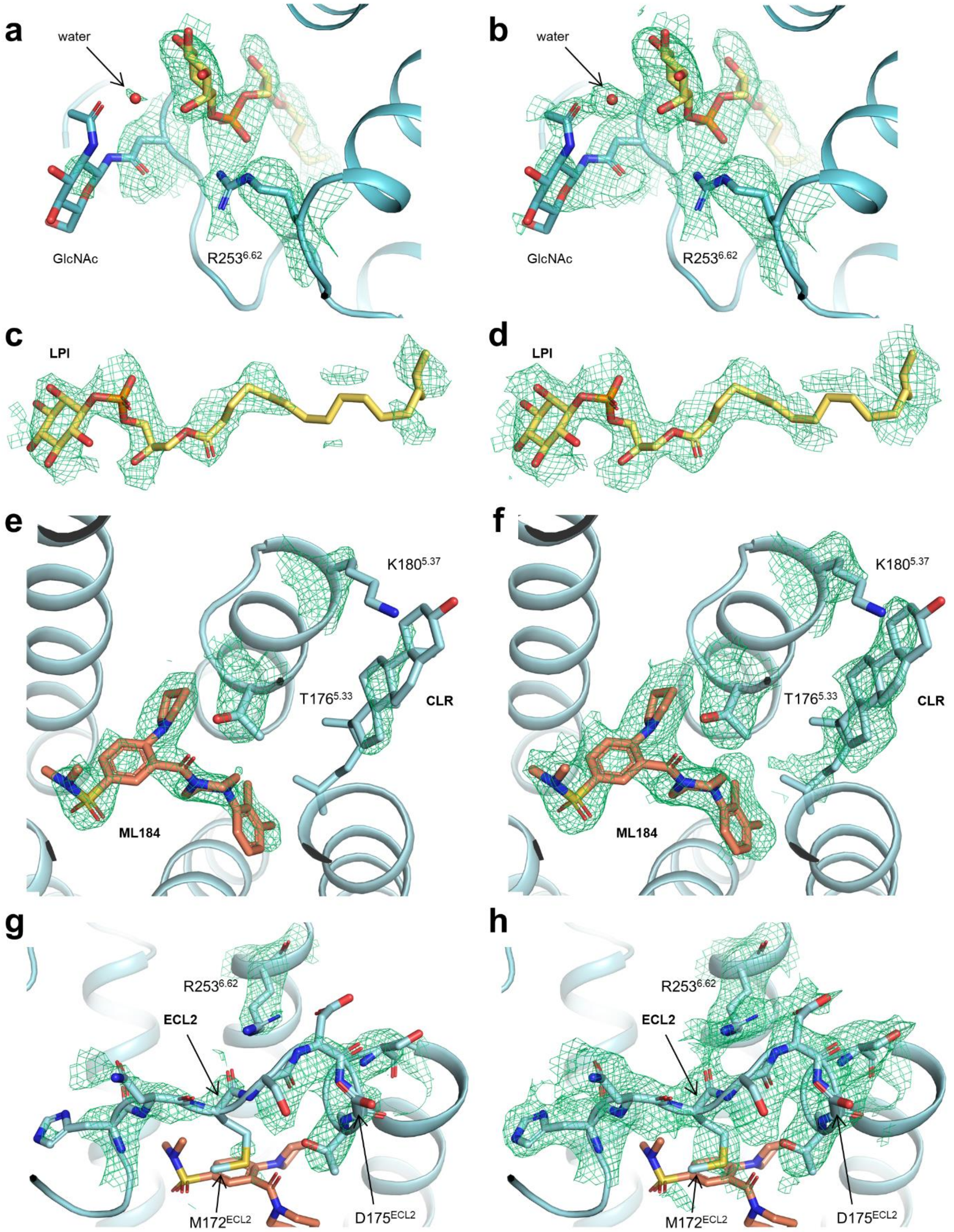


**Supplementary Fig. S3. Cryo-EM Map of ligand binding pockets and ECL2 residues. a, b** Cryo-EM map of the extracellular ends of LPI, GlcNAc, N171, and R253 at two different contour levels. **c, d** Cryo-EM map of LPI at two different contour levels. **e, f** Cryo-EM map of ML184, T176, CLR, and K180 at two different contour levels. **g, h** Cryo-EM map of ECL2 residues between S178 and H170 and R253 of the ML184 structure at two different contour levels.

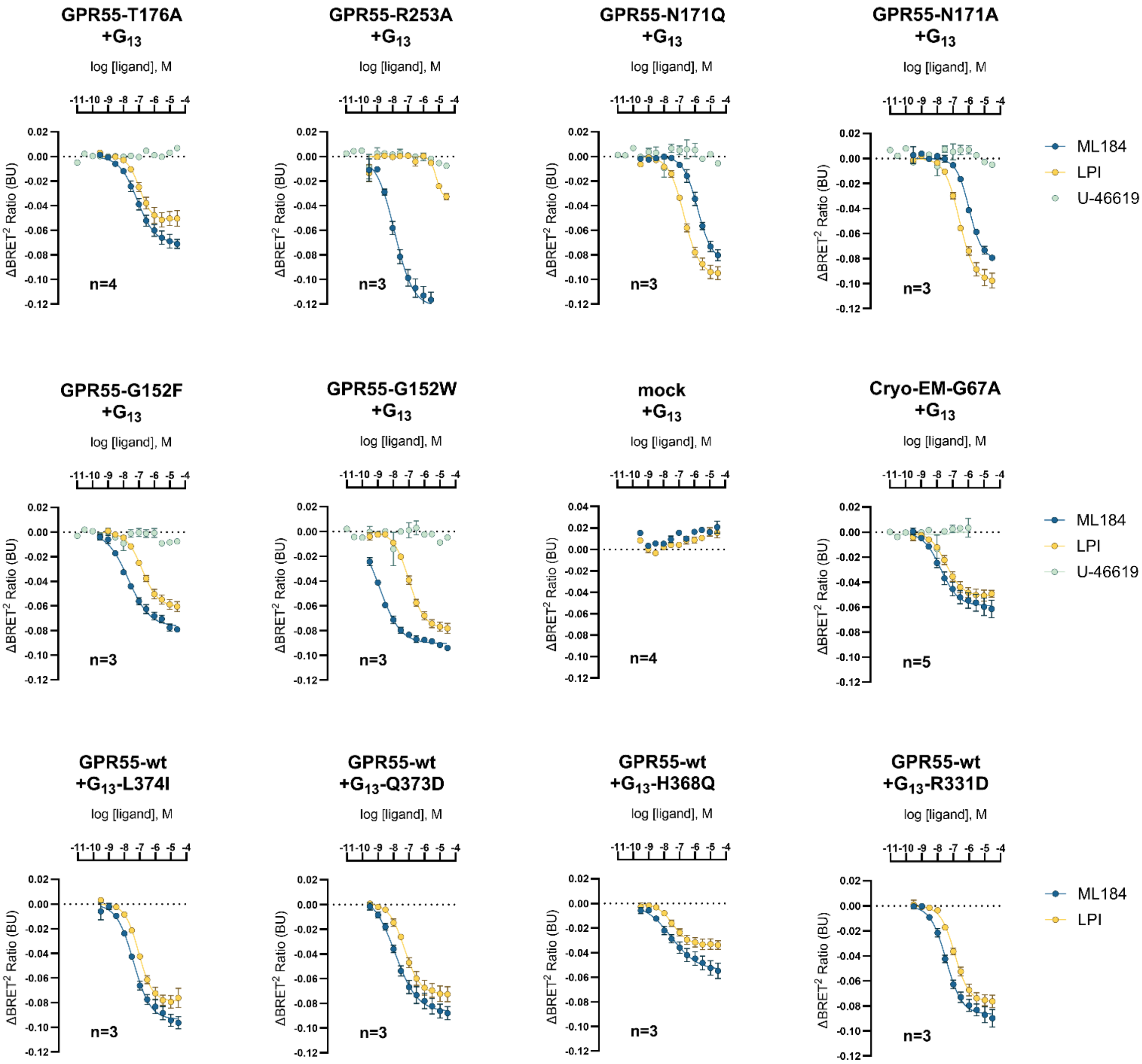


**Supplementary Fig. S4. Dose-response curves of G protein dissociation assays.** Data points represent means ± SEM from 3-7 independent experiments as indicated in Supplementary Table S3. Data of the negative control ligand U-46619 at GPR55 mutants represent means ± SEM from only two independent experiments.

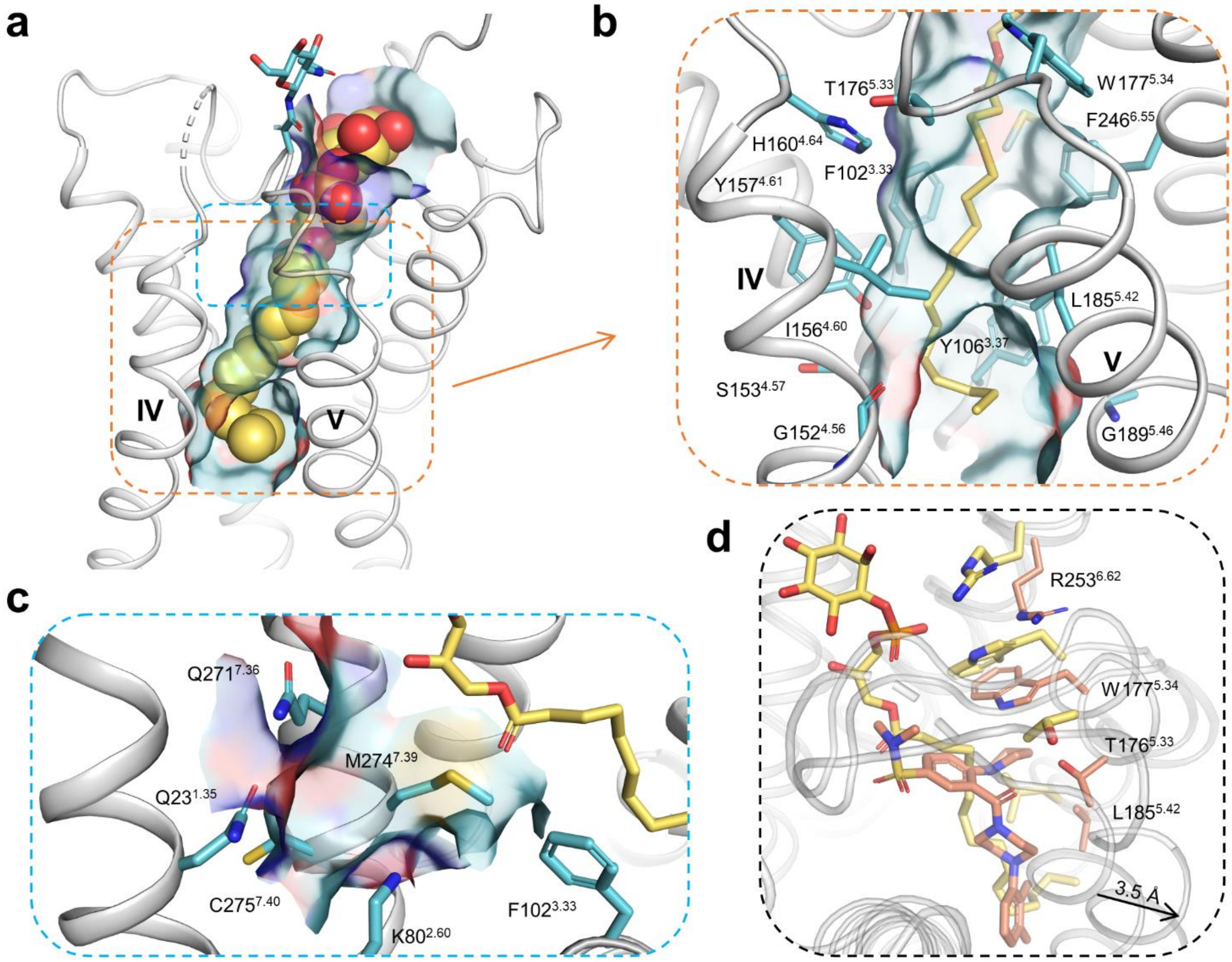


**Supplementary Fig. S5. Location of LPI and the palmitoyl-tail in the ligand binding pocket. a** Overview of the binding position of LPI (yellow spheres) in GPR55. **b** Magnified image of the binding pocket of the lipophilic palmitoyl-tail of LPI (yellow sticks) in the binding channel highlights the contacting amino acids. The binding pocket surface of LPI is shown in cyan in both panels. **c** Magnified image of the receptor cavity facing the glycerol hydroxy group. **d** Structural comparison of the binding pockets of LPI (yellow sticks) and ML184 (salmon sticks) shows rearrangements of several residues and an outward movement of the extracellular end of helix V to accommodate ML184.

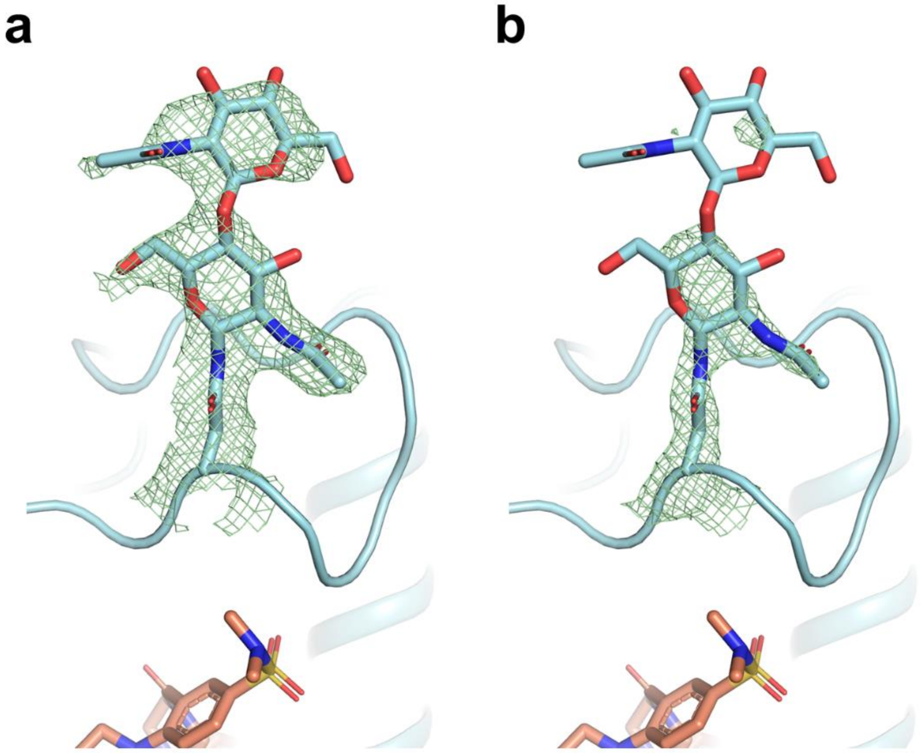


**Supplementary Figure S6. N-linked glycosylation in the GPR55-ML184-structure with two initial GlcNAc units. a** and **b** Cryo-EM map of N171$^{ECL2}$ and the adjacent two glycan units are displayed with green mesh at different contour levels.

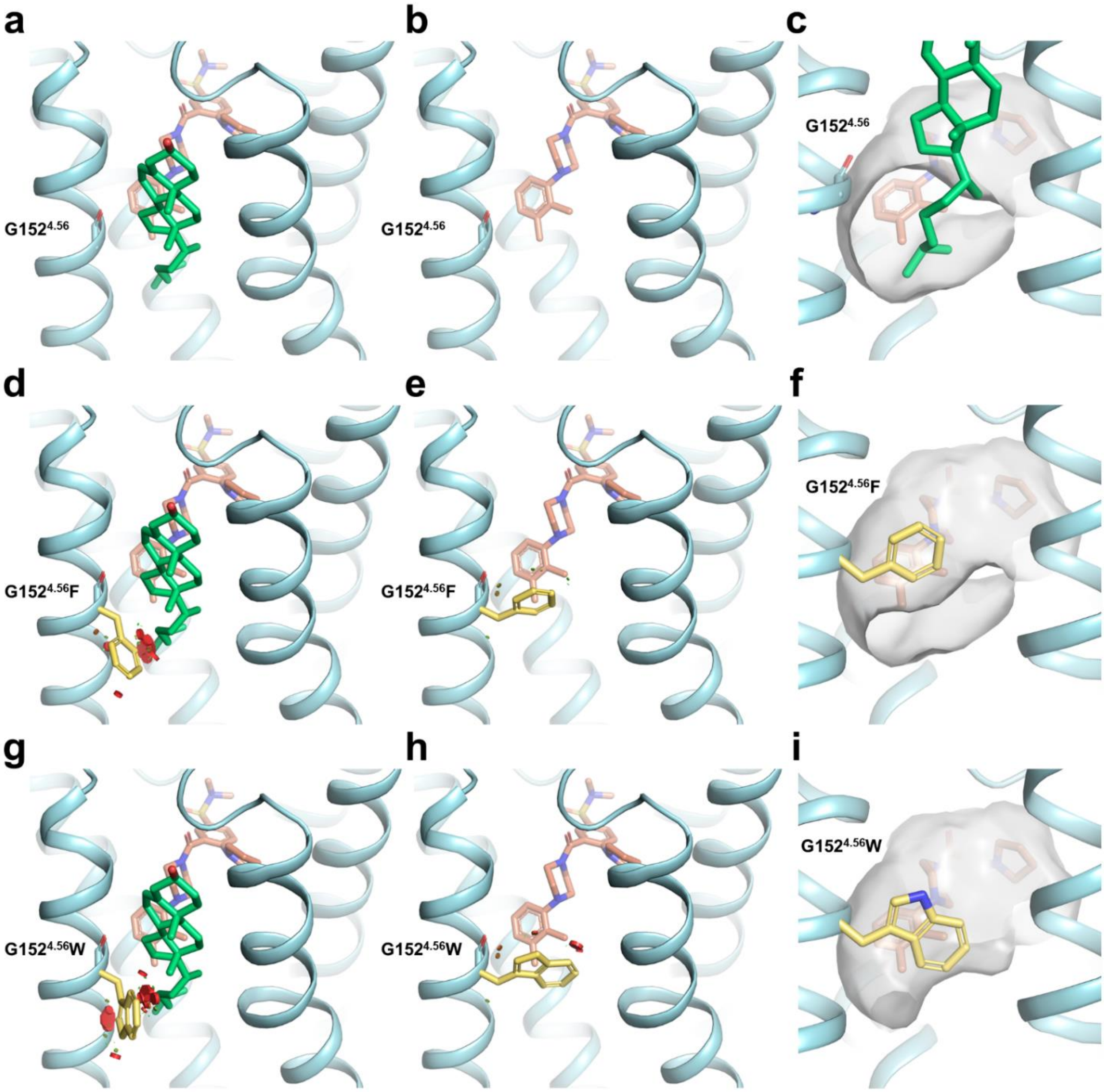


**Supplementary Fig. S7. Models of G152 single point mutations in the membrane opening.** The figure shows the membrane opening between helices IV and V **a, d, g** with CLR (green sticks) present and clashes displayed, **b, e, h** with CLR removed and clashes displayed, and **c, f, i** wt receptor or final models with ML184 (salmon sticks) surface displayed in gray. **a – c** shows the native receptor without mutation, **d – f** shows the receptor with G152$^{4.56}$F mutation, and **g – i** shows the receptor with G152$^{4.56}$W mutation (side chains shown as yellow sticks). Red disks indicate steric clashes. Point mutations of G152$^{4.56}$ to either F or W were introduced using PyMOL.

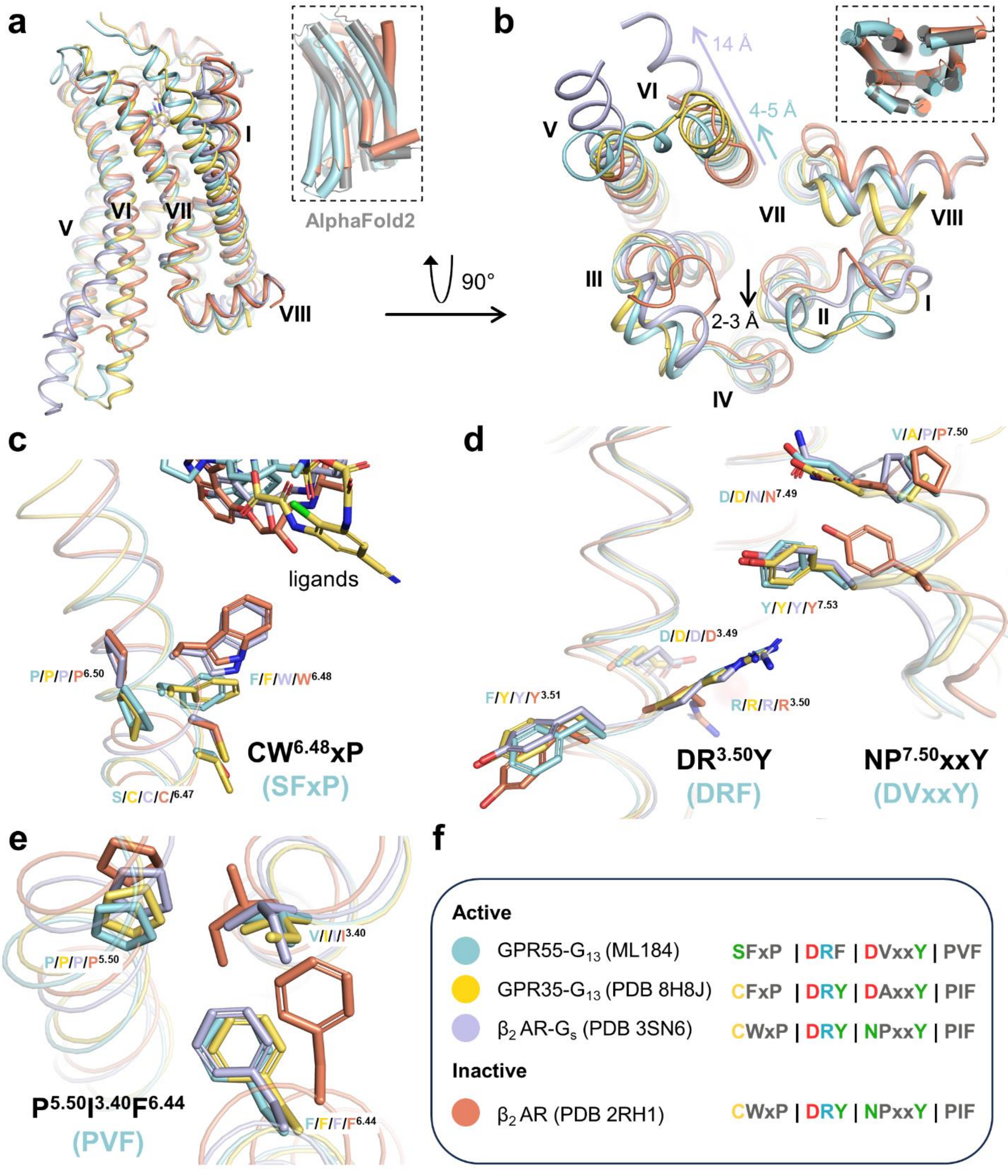


**Supplementary Fig. S8. Comparison of conserved activation microswitches.** Superimposition of GPR55-$G_{13}$ (active structure, blue), GPR35-$G_{13}$ (active structures, yellow, PDB 8H8J), $\beta_2$ adrenergic receptor (active structure, violet, PDB 3SN6), $\beta_2$AR (inactive structure, orange, PDB 2RH1). An inactive state AlphaFold model from GPCRdb (gray) is superimposed separately (rectangle box) with GPR55 and the inactive $\beta_2$AR using a cylindrical helix representation. **a** Alignment focused on the transmembrane helices. **b** Intracellular view of the helix bundle highlights minor outward helix IV outward movement of GPR55 in comparison to the inactive state structure. Different activation microswitches were compared focused on **c** CWxP motif, **d** DRY and NPxxY motif, and **e** PIF motif. **f** Color coding and sequence alignment of compared microswitches between all four receptors.

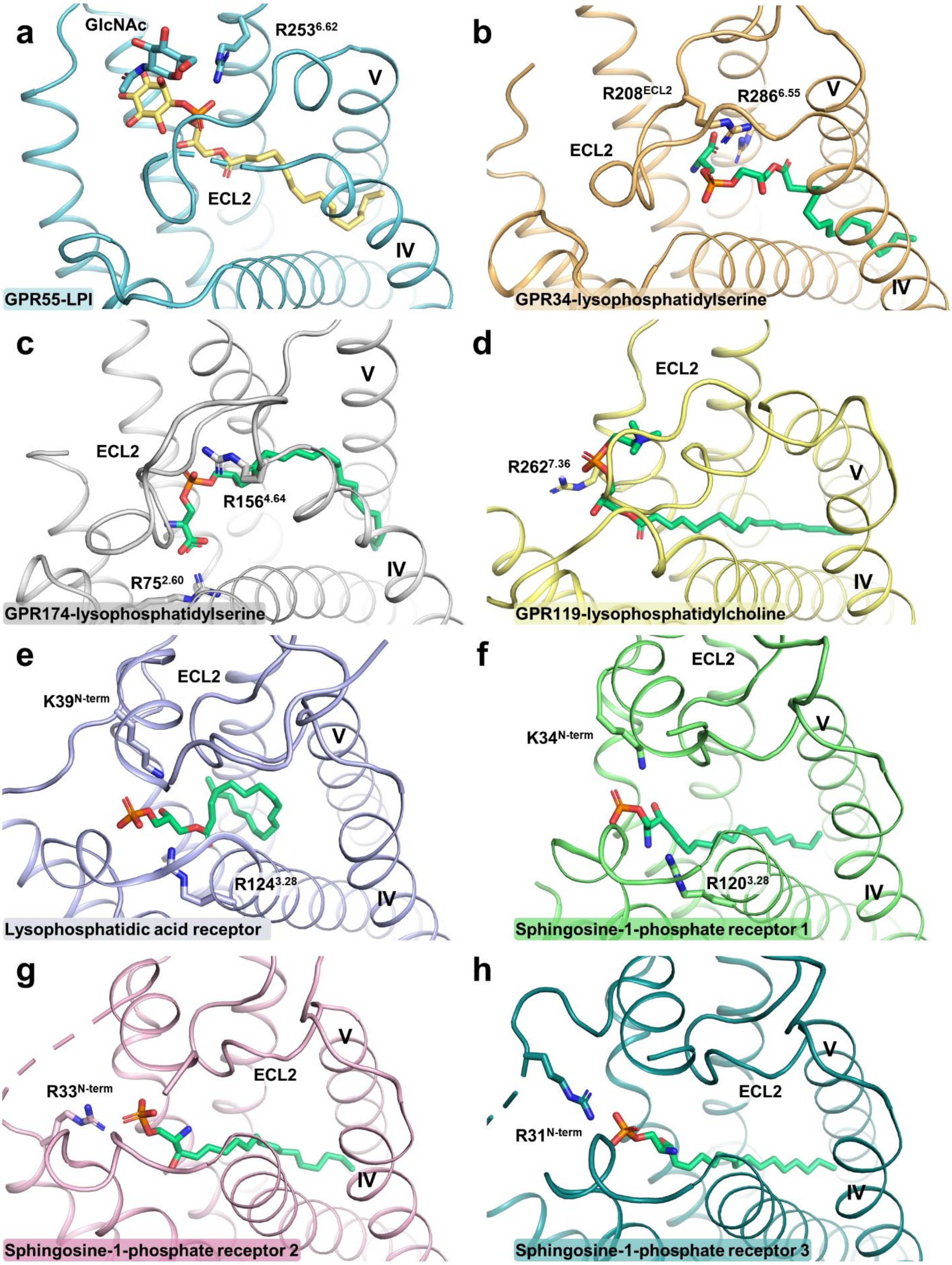


**Supplementary Fig. S9. Ligand recognition of selected different lipid receptors through their negatively charged moieties.** GPCR-lipid interactions of **a** GPR55-LPI (this study), **b** GPR34-LPS (PDB 8SAI), **c** GPR174-LPS (PDB 7XV3), **d** GPR119-LPC (PDB 7XZ5), **e** $LPAR_1$-LPA (PDB 7TD0), **f – h** and $S1P_{1-3}$-S1P (PDB 7VIE, 7T6B, and 7EW3). The same perspective was used for all binding pockets.

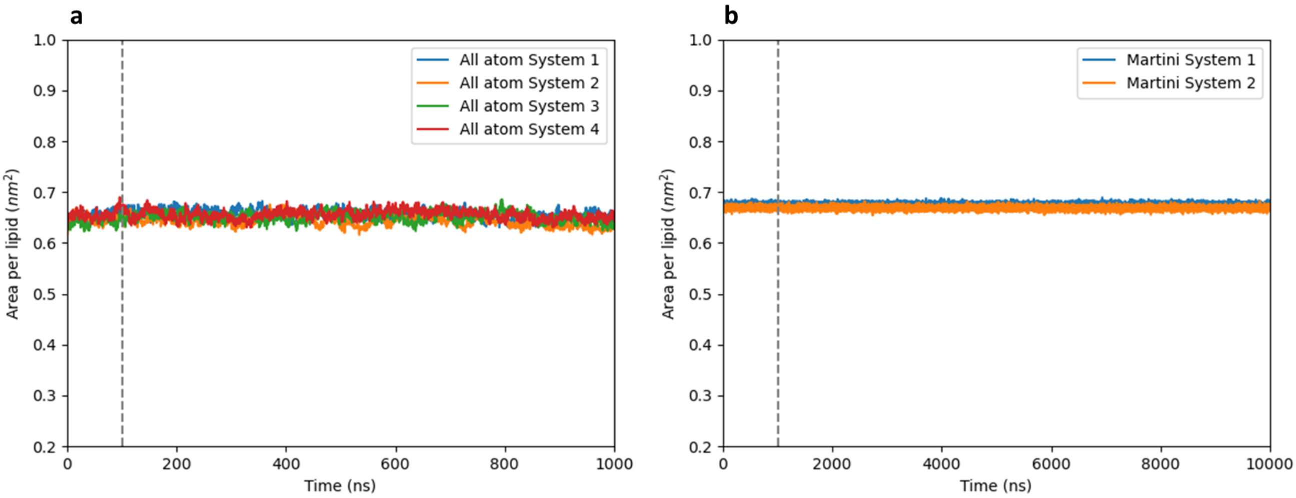


**Supplementary Fig. S10. Equilibration status of molecular dynamics (MD) simulations.** The equilibration of the MD systems is illustrated by a plot showing the area per lipid over time for the all-atom **a**, and martini simulations **b**. The naming conventions for the systems align with those detailed in the Methods section. The area per lipid is calculated as simulation box dimension x, multiplied by simulation box dimension y and divided by the number of DOPC and Cholesterol molecules in a single leaflet of lipid bilayer. **a** The all-atom simulations were conducted over a period of 1 microsecond (µs), with the initial 100 nanoseconds (ns) serving as the equilibration phase. The subsequent 900 ns were used for analysis. A dotted vertical line marks the transition from equilibration to analysis. **b** In case of the martini simulations, the first 1 µs was dedicated to equilibration, followed by a 9 µs period for analysis. The transition from equilibration to analysis is indicated by a dotted vertical line.

**Supplementary Table S1. List of GPCR structures determined in complex with $G\alpha_{12}$ or $G\alpha_{13}$ proteins as of July 2024.**

| **Receptor** | **Abbreviation** | **Family** | **G protein subtype** | **Ligand** | **PDB ID** | **FSC Resolution** |
|---|---|---|---|---|---|---|
| Adhesion G protein-coupled receptor L3 | AGRL3 | Adhesion | $G\alpha_{13}$ | apo | 7SF7 | 2.90 Å |
| Adhesion G protein-coupled receptor G1 | AGRG1 | Adhesion | $G\alpha_{13}$ | apo | 7SF8 | 2.70 Å |
| Sphingosine-1-phosphate receptor 2 | $S1P_2R$ | Rhodopsin | $G\alpha_{13}$ | S1P | 7T6B | 3.19 Å |
| Adhesion G protein-coupled receptor F1 | AGRF1 | Adhesion | $G\alpha_{13}$ | apo | 7WY0 | 2.83 Å |
| Adhesion G protein-coupled receptor F1 | AGRF1 | Adhesion | $G\alpha_{12}$ | apo | 7WZ7 | 2.83 Å |
| Adhesion G protein-coupled receptor L3 | AGRL3 | Adhesion | $G\alpha_{12}$ | apo | 7X10 | 2.93 Å |
| Adhesion G protein-coupled receptor E5 | AGRE5 | Adhesion | $G\alpha_{13}$ | apo | 7YDH | 3.10 Å |
| Adhesion G protein-coupled receptor E5 | AGRE5 | Adhesion | $G\alpha_{12}$ | apo | 7YDJ | 3.03 Å |
| GPR35 | GPR35 | Rhodopsin | $G\alpha_{13}$ | lodox-amide | 8H8J | 3.20 Å |
| GPR55 (this publication) | **GPR55** | **Rhodopsin** | $\mathbf{G\alpha_{13}}$ | **LPI** | **9GE3** | **2.96 Å** |
| GPR55 (this publication) | **GPR55** | **Rhodopsin** | $\mathbf{G\alpha_{13}}$ | **ML184** | **9GE2** | **2.64 Å** |

**Supplementary Table S2. Cryo-EM data collection, refinement and validation statistics.**

| | **GPR55-Gα$_{13}$β$_1$γ$_2$-ScFv16-LPI** (PDB 9GE3) | **GPR55-Gα$_{13}$β$_1$γ$_2$-ScFv16-ML184** (PDB 9GE2) |
|---|---|---|
| **Data collection and processing** | | |
| Magnification | 130,000 | 105,000 |
| Voltage (kV) | 300 | 300 |
| Detector | Falcon IV | Gatan K3 |
| Electron exposure ($e^-/Å^2$) | 40 | 45 |
| Defocus range (μm) | -2.54 to -0.40 | -3.56 to -0.88 |
| Pixel size (Å) | 0.951 | 0.829 |
| Symmetry imposed | C1 | C1 |
| Initial particle images (no.) | 5,188,047 | 13,541,164 |
| Final particle images (no.) | 397,853 | 829,193 |
| Map resolution (Å)* FSC threshold 0.143 | 2.87 (composite map)<br>2.96 (consensus map)<br>3.01 (focused map GPCR)<br>2.88 (focused map G protein) | 2.51 (composite map)<br>2.64 (consensus map)<br>2.77 (focused map GPCR)<br>2.51 (focused map G protein) |
| **Refinement** | | |
| Initial model used (PDB code) | ML184 structure | AlphaFold (GPR55) & 7YDH |
| Map sharpening *B* factor ($Å^2$) | 109.2 (consensus map)<br>115.6 (focused map GPCR)<br>96.4 (focused map G protein) | 98.6 (consensus map)<br>102.5 (focused map GPCR)<br>87.5 (focused map G protein) |
| Model composition | | |
| Non-hydrogen atoms | 8,563 | 9,082 |
| Protein residues | 1,078 | 1,137 |
| Ligands (lipids) | 1 (0) | 1 (1) |
| Waters | 6 | 15 |
| *B* factors ($Å^2$) | | |
| Protein | 49.3 | 37.5 |
| Ligand | 29.6 | 17.2 |
| RMSD | | |
| Bond lengths (Å) | 0.002 | 0.003 |
| Bond angles (°) | 0.474 | 0.535 |
| Validation | | |
| MolProbity score | 1.95 | 1.70 |
| Clashscore | 8.86 | 5.11 |
| Poor rotamers (%) | 3.07 | 2.82 |
| Ramachandran plot | | |
| Favored (%) | 97.46 | 97.60 |
| Allowed (%) | 2.54 | 2.40 |
| Disallowed (%) | 0 | 0 |

**Supplementary Table S3. G protein dissociation assay results.***

| Receptor/ Mutant | G protein | Basal activation ± SEM (%) | Ligand | $pEC_{50}$ ± SEM | Adjusted P value vs. wt† | Efficacy ± SEM (%) | No. of independent experiments |
|---|---|---|---|---|---|---|---|
| **wt GPR55** | $G\alpha_{13}$ | 66 ± 2 | ML184 | 7.35 ± 0.07 | n.a. | 100 ± 2 | 7 |
| | | | LPI | 7.45 ± 0.08 | n.a. | 86 ± 2 | 7 |
| **wt GPR55** | $G\alpha_{12}$ | 13 ± 5 | ML184 | n.d. | n.a. | n.d. | 4 |
| | | | LPI | n.d. | n.a. | n.d. | 4 |
| **Cryo-EM construct** | $G\alpha_{13}$ | 49 ± 6 | ML184 | 7.74 ± 0.03 | 0.0010 | 86 ± 2 | 5 |
| | | | LPI | 7.40 ± 0.06 | 0.9968 | 82 ± 4 | 5 |
| **T176A** | $G\alpha_{13}$ | 50 ± 1 | ML184 | 7.11 ± 0.08 | 0.0377 | 100 ± 1 | 4 |
| | | | LPI | 6.96 ± 0.02 | 0.0001 | 87 ± 2 | 4 |
| **R253A** | $G\alpha_{13}$ | 13 ± 3 | ML184 | 7.84 ± 0.08 | 0.0005 | 103 ± 3 | 3 |
| | | | LPI | 5.17 ± 0.09 | <0.0001 | 37 ± 2 | 3 |
| **N171Q** | $G\alpha_{13}$ | 19 ± 2 | ML184 | 5.85 ± 0.07 | <0.0001 | 76 ± 2 | 3 |
| | | | LPI | 6.72 ± 0.08 | <0.0001 | 85 ± 3 | 3 |
| **N171A** | $G\alpha_{13}$ | 16 ± 3 | ML184 | 5.98 ± 0.04 | <0.0001 | 73 ± 3 | 3 |
| | | | LPI | 6.61 ± 0.06 | <0.0001 | 85 ± 3 | 3 |
| **G152F** | $G\alpha_{13}$ | 52 ± 3 | ML184 | 7.66 ± 0.06 | 0.0375 | 108 ± 3 | 3 |
| | | | LPI | 6.79 ± 0.02 | <0.0001 | 94 ± 3 | 3 |
| **G152W** | $G\alpha_{13}$ | 41 ± 2 | ML184 | 8.87 ± 0.01‡ | <0.0001 | 107 ± 1 | 3 |
| | | | LPI | 7.00 ± 0.03 | 0.0009 | 96 ± 5 | 3 |
| **TBXA2** | $G\alpha_{13}$ | -15 ± 14 | U-46619 | 9.03 ± 0.11 | n.a. | 100 ± 2 | 3 |
| | $G\alpha_{12}$ | -6 ± 15 | U-46619 | 7.62 ± 0.15 | n.a. | 100 ± 8 | 3 |
| **wt GPR55** | $G\alpha_{13}$-L374I | 17 ± 3 | ML184 | 7.44 ± 0.05 | 0.8504 | 84 ± 1 | 3 |
| | | | LPI | 7.09 ± 0.07 | 0.0121 | 71 ± 3 | 3 |
| | $G\alpha_{13}$-Q373D | 33 ± 11 | ML184 | 7.77 ± 0.04 | 0.0058 | 94 ± 7 | 3 |
| | | | LPI | 7.28 ± 0.01 | 0.3500 | 84 ± 8 | 3 |
| | $G\alpha_{13}$-H368Q | 64 ± 8 | ML184 | 7.53 ± 0.09 | 0.3466 | 101 ± 4 | 3 |
| | | | LPI | 7.45 ± 0.03 | >0.9999 | 88 ± 6 | 3 |
| | $G\alpha_{13}$-R331D | 27 ± 7 | ML184 | 7.47 ± 0.10 | 0.6846 | 89 ± 3 | 3 |
| | | | LPI | 6.92 ± 0.01 | 0.0005 | 80 ± 4 | 3 |

*The degree of activation in % was calculated by normalization of $BRET^2$ ratios ($BRET^2$ ratio of 30 μM ligand for efficacy or basal $BRET^2$ ratios of 1.5% DMSO) to the respective $BRET^2$ ratios for the wt GPR55 plus $G_{13}$-biosensor at 30 μM ML184 (100% activation) and for a mock-transfection plus $G_{13}$-biosensor (0% activation). The same normalization approach was used for the $G\alpha_{13}$ mutants.

†P values were calculated by one-way ANOVA with Dunnett's post-hoc test for all mutants versus wt GPR55 separately for each ligand (seven comparisons each). The ANOVA P values equal <0.0001 for both ligand comparisons. The $G\alpha_{13}$ mutants were tested independently versus wt GPR55 plus wt $G\alpha_{13}$. Here, the ANOVA P value equals 0.0237 for the ML184 comparison and 0.0008 for the LPI comparison, respectively.

‡The $pEC_{50}$ value of ML184 at GPR55 mutant G152W was calculated by extrapolating $\Delta BRET^2$ ratios for concentrations <0.3 nM. n.d.: not determined. n.a. not applicable

**Supplementary Table S4.** GPCR structures with resolved N- or O-linked glycosylation in the PDB as of July 2024.

| PDB ID | Receptor | Ligand distance within 5 Å | Residue(s) | Location | Glycan units |
|---|---|---|---|---|---|
| **Class A GPCRs** | | | | | |
| **9GE2, 9GE3 (this publication)** | **GPR55** | **Yes** | **N171** | **ECL2** | **1-2** |
| 2J4Y, 3C9M, 3PQR, 6FKB, 6FUF, 7ZBC, 7ZBE | Rhodopsin | no | N2<br>N15 | *N*-term | 0-1<br>1-4 |
| 3V2W, 3V2Y, 7EVY, 7TD3, 7TD4 | $S1PR_1$ | no | N30 | *N*-term | 1 |
| 7YXA | $S1PR_5$ | no | N20 | *N*-term | 1 |
| 7SRQ, 7SRS | Serotonin $5\text{-}HT_{2B}$ receptor | no | N204 | ECL2 | 1 |
| 6DO1, 6OS2 | Angiotensin II receptor type 1 | no | N176 | ECL2 | 1 |
| 6MEO | Chemokine receptor type 5 | no | S7 | *N*-term | 1 |
| 7RKF | US28 | no | N9 | *N*-term | 1 |
| **Class B GPCRs** | | | | | |
| 5NX2, 6LN2 | Glucagon-like peptide 1 | no | N63<br>N82 | *N*-term | 0-1<br>2 |
| 5XEZ, 5XF1 | Glucagon receptor | no | N46<br>N59<br>N74<br>N78 | *N*-term | 1<br>2-3<br>2<br>2 |
| 7TYF, 7TYI, 7TYN, 7TYO, 7TYX, 7TYW, 7TZF, 8F0J, 8F0K, 8F2A, 8F2B, 9AUC | Calcitonin and Amylin 1-3 receptors | no | N73<br>N125<br>N130 | *N*-term | 0-1<br>0-1<br>1 |
| **Class C GPCRs** | | | | | |
| 6N51, 6N52, 7FD8, 7FD9 | Metabotropic glutamate receptor 5 | no | N210<br>N445 | *N*-term | 1<br>0-1 |
| **Class F GPCRs** | | | | | |
| 5L7D, 5L7I, 5V56, 7ZI0 | Smoothened receptor | no | N188<br>N493 | *N*-term<br>6.74 | 0-1<br>0-1 |